IOP Publishing Smart Materials and Structures
Smart Mater. Struct. **26** (2017) 045010 (11pp) https://doi.org/10.1088/1361-665X/aa5fe3

Efficient and robust nonlinear model for smart materials with application to composite magnetostrictive plates

Hafez Tari[1], Sushma S Santapuri[2] and Marcelo J Dapino[1]

[1] Department of Mechanical and Aerospace Engineering, The Ohio State University, Columbus, OH 43210, United States of America
[2] Department of Applied Mechanics, Indian Institute of Technology Delhi, New Delhi, India 110016

E-mail: tari.1@osu.edu, ssantapuri@am.iitd.ac.in and dapino.1@osu.edu

Received 31 July 2016, revised 6 February 2017
Accepted for publication 10 February 2017
Published 7 March 2017

Abstract

This paper presents a computationally efficient and robust nonlinear modeling framework for smart materials. The framework describes a smart material system through a new 3D inversion scheme for coupled nonlinear constitutive equations which can be integrated with the variational form of governing equations. Building on the Newton technique, the inversion scheme can be applied to any nonlinear smart material with a differentiable direct constitutive model. To further improve computational efficiency, the inversion scheme is integrated with a reduced dimensional (2D) model for smart composite structures. The resulting coupled 2D framework is applied to an aluminum-Galfenol composite plate that operates in actuation mode, and is solved using multiphysics finite element software. Major and minor magnetostriction curves are obtained for the actuator displacements at the tip of the Galfenol element by applying unbiased and biased magnetic fields. A significant advantage in numerical convergence and computational time, an almost six-time speedup for a dynamic simulation case, is demonstrated via comparison with an existing approach for magnetostrictive material modeling. The framework is suitable for fast design and optimization of nonlinear smart material structures.

Keywords: inverse model, active composite plates, iron-gallium alloys, Galfenol, constitutive model, magnetostriction

(Some figures may appear in colour only in the online journal)

1. Introduction

Smart materials exhibit controllable changes in shape and properties in response to external stimuli. Such changes are accompanied with coupling of different physical effects and conversion of energy from one type to another. For instance, piezoelectric and electrostrictive materials convert electrical energy to mechanical energy and vice versa; magnetostrictive materials exhibit coupling of magnetic and mechanical effects; shape-memory alloys and polymers respond to thermal activation by changing their crystal structure and macroscopic dimensions; and pH sensitive polymers swell in response to changes in external pH. The coupling of physical effects in smart materials enables tuning of material properties, thus making smart materials attractive for design of sensors [1], actuators [2], energy harvesters [3], and vibration controlling devices [4]. See [5, 6] for more information on smart materials.

Smart materials typically exhibit nonlinear and hysteretic behavior, even though certain smart materials can be characterized using linear models within a specified operational regime. For instance, piezoelectric materials like PZT, PVDF, and $BaTiO_3$, when poled, exhibit approximately linear behavior for low to moderate inputs [7]. Within a specified, restricted operating regime, these linear constitutive models (e.g., [8]) are beneficial for efficient transducer design. However, smart materials like magnetostrictives, electrostrictives, and shape memory materials exhibit higher order of

nonlinearity and hysteresis, which cannot be adequately described with linear constitutive models.

Magnetostrictive materials are a class of smart materials that exhibit nonlinear magnetomechanical coupling. These materials undergo dimensional changes when exposed to a magnetic field, and conversely, exhibit changes in magnetization when subjected to mechanical stresses. Two common magnetostrictive materials are terbium-dysprosium-iron (Terfenol-D) and iron-gallium (Galfenol). Terfenol-D produces relatively large magnetostriction (≈1600 ppm) at a moderate magnetic field (≈200 kA m^{-1}), making it well suited for actuator designs; see for example Chakrabarti and Dapino [9]. Because Terfenol-D is brittle, it always requires stress biasing to avoid tension. On the other hand, Galfenol exhibits moderate magnetostriction (≈350 ppm) at low magnetic fields (≈8 kA m^{-1}), possesses high tensile strength (≈500 MPa), and experiences a limited variation in magnetomechanical properties for temperatures between −20 °C and 80 °C (see [10]). When composed of less than 20 at.% gallium, Galfenol retains the machinability and ductility of iron. As such, it can be produced in sheets or wires, as well as welded, threaded or extruded into unprecedented 3D structures that are both active and load-bearing.

The intrinsic nonlinearity and hysteresis manifested by magnetostrictive materials and other nonlinear smart materials necessarily result in complex transducer models. Several methods exist that can efficiently model nonlinear coupled systems. At one extreme, *phenomenological* approaches fit a curve or surface to measurement data, which provides efficiency but ignores the underlying physics. At the other extreme, *microscopic models* provide an accurate description of the physical phenomena by considering all possible energies. However, owing to their relative complexity, these models are often associated with high computational cost and require sophisticated computational techniques for analysis. For instance, Pérez-Aparicio and Sosa [11] presented a fully coupled, three-dimensional finite element algorithm for magnetostrictive materials based on a continuum physics formulation that takes nonlinear and dynamic effects into account through Maxwell stress tensor and equation of motion. Also, several techniques were proposed in micromagnetics to solve the Landau–Lifshitz equation [12] that describes the evolution of magnetization in a ferromagnetic material. To this end, a Gauss-Seidel projection method was proposed by Wang *et al* [13] and a boundary-corrected algorithm for general geometries was developed by García-Cervera *et al* [14]. Built on a fast multipole method, Van de Wiele *et al* [15] presented a numerical finite difference scheme that employs far and near field interactions to describe the interactions between finite difference cells.

Finally, a third kind of approach, *macroscopic modeling*, uses an intermediate approach by relating the macroscopic response of a material to simplified descriptions of its microscopic behavior. Macroscopic models, therefore, strike a balance between computational speed, accuracy, and predictive ability. For magnetostrictive materials, in particular, classical macroscopic models include the Preisach model [16], Globus model [17], Jiles-Atherton model [18], and Stoner-Wohlfarth model [19]. These models are compared in detail in [20]. For Terfenol-D, Carman and Mitrovic [21] formulated a model by expanding the Gibbs free energy in a truncated Taylor series, the coefficients of which were determined experimentally. Zheng and Sun [22] included higher order terms in the expansion to improve the applicability of the model for larger magnetic field inputs. Armstrong [23] proposed an incremental hysteretic magnetoelastic constitutive theory of pseudo-cubic magnetostrictive alloys that can be applied to Terfenol-D and, with some modifications, to Galfenol. The bulk magnetization and magnetostriction are calculated from the expected values of a large collection of magnetic moments. The probability density function is a Boltzmann distribution, where minimum energy orientations are more probable. The Armstrong model is computationally intensive, as it searches for global energy minima. Atulasimha *et al* [24] improved efficiency by considering only 98 fixed orientations. Evans and Dapino [25] greatly enhanced the computational speed by formulating the energy functions around local minima along Galfenol's six easy crystallographic directions. The computational cost of this model was further reduced by Chakrabarti [26].

In characterization of smart materials, intensive physical quantities such as stress and magnetic field are often used as independent variables. Extensive conjugate quantities such as strain and magnetic flux density are used as dependent variables. The macroscopic constitutive models described above follow this scheme, and we refer to these models as the direct models (in a mathematical sense). However, in certain design and control situations, inverse models are necessary, wherein stresses must be determined from specified magnetic fields and strains. This inversion typically involves an iterative procedure, and requires sophisticated criteria to find physical solutions, especially, when multiple mathematical solutions exist. Chakrabarti and Dapino [27] proposed an inverse model that describes the full nonlinear coupling in 3D Galfenol transducers. However, this model is susceptible to convergence issues, which are drastically alleviated by further developments presented by Deng and Dapino [28]. Nonetheless, both of these models are built on the direct model given in [26], which is prone to singularities. These can burden computation, especially when the model is integrated into finite element solvers. Tari *et al* [29] addressed this shortcoming through a reformulation of this direct model with an exact solution procedure.

In addition, much effort has recently been devoted to developing sophisticated 3D nonlinear models that improve the accuracy and scope of the transducer devices built with such materials, as in [30–32]. However, for certain geometries and applications, reduced dimensional constitutive models are both sufficiently accurate and computationally efficient. For instance, Mindlin [33] developed a first-order plate theory for high frequency piezoelectric crystals. Reddy [34] developed a third order plate theory for laminated composites with integrated sensors and actuators that works reasonably well even for thick composites. Kannan and Dasgupta [35] presented a two-dimensional, quasi-static, finite-element scheme to model nonlinear magnetostrictive material systems. Datta *et al* [36, 37]

used classical laminated plate theory with the Armstrong model to characterize laminated sensors and actuators in the absence of current-induced magnetic fields. As far as capturing the dynamic behavior of smart materials, Shu *et al* [38] recently developed a 1D nonlinear model that simulates the dynamic response of Galfenol-driven unimorph actuators.

In this paper, we develop a computational framework that consists of a globally convergent inverse model, which can effectively and efficiently solve for system unknowns in a finite element scheme to design smart material systems. The inversion scheme is general, and can be applied to any nonlinear smart material with a given direct model. To illustrate the model, Galfenol is taken as an example, and analytical Jacobian terms corresponding to the direct model developed by Tari *et al* [29] are derived. Subsequently, this model is integrated with a finite element software to model a magnetostrictive material based composite actuator with thin plate geometry. Utilizing a reduced 2D formulation for this application, we demonstrate the improvement in computational efficiency and numerical robustness.

The rest of the paper is organized as follows. In the following section, a 3D system model for embedded smart composites is studied, and an inverse system model for smart materials is presented. A recent magnetomechanical direct model is reviewed in section 3 for which the exact strain derivative terms are derived analytically in section 4. A reduced 2D system model for embedded smart composites is given in section 5. To demonstrate the computational framework, a Galfenol-aluminum plate actuator is considered as a case study in section 6, and the simulation results are given accordingly. Finally, discussions and conclusions are given.

2. 3D system model for embedded smart composites

Consider a composite structure consisting of (i) smart material domain, i.e., an *active domain* and (ii) non-smart material domain, i.e., a *passive domain*. The structural behavior of the composite is governed by 3D Navier's equation along with constitutive equations that describe the material behavior specific to each domain. Referring, for example, to [30], the 3D weak form of Navier's equation is

$$\int_{V_{\text{tot}}} \left[\rho \frac{\partial^2 \mathbf{u}}{\partial t^2} \cdot \delta \mathbf{u} + c \frac{\partial \mathbf{u}}{\partial t} \cdot \delta \mathbf{u} + \mathbf{T} \cdot \delta \mathbf{S} \right] \mathrm{d}V = \int_{\partial V_{\text{tot}}} \mathbf{t} \cdot \delta \mathbf{u} \, \mathrm{d}\partial V + \int_{V_{\text{tot}}} \mathbf{f}_B \cdot \delta \mathbf{u} \, \mathrm{d}V, \tag{1}$$

where t is the time, ρ is the density, c represents the damping coefficient, and $\mathbf{T}$ and $\mathbf{f}_B$ denote, respectively, the stress tensor and external body force acting on the domain V_{tot}; the traction vector $\mathbf{t}$ acts on the boundary ∂V_{tot}; and $\mathbf{S}$ and $\mathbf{u}$ represent, respectively, the strain tensor and displacement vector at each point in the domain V_{tot} with the fact that

$$\mathbf{S} = \frac{1}{2}(\nabla \mathbf{u} + \nabla \mathbf{u}^{\mathrm{T}}). \tag{2}$$

Stresses are evaluated using material specific constitutive equations. The passive domain (typically non-magnetic metals such as steel, brass, and aluminum) is governed by Hooke's law, i.e.,

$$\mathbf{T}_p = \mathbf{C}_p \mathbf{S}_p, \tag{3}$$

where the subscript p signifies the passive domain, and $\mathbf{C}_p$ is the second rank modulus tensor.

Experimentally, active materials are controlled by field (e.g., electric field, magnetic field, or temperature gradient) and stress as independent variables, and flux density (e.g., current density, magnetic flux, or entropy) and strain are measured as dependent variables. We refer to the constitutive models that follow this scheme as direct models, and write, for example, the constitutive model for strain in the general form

$$\mathbf{S}_a = \mathbf{S}(\boldsymbol{\mathcal{F}}, \mathbf{T}_a), \tag{4}$$

where $\mathbf{S}_a$ and $\mathbf{T}_a$ are the strain and stress in the active domain; and $\boldsymbol{\mathcal{F}}$ represents the external field vector that can include quantities such as electric field, magnetic field, or temperature gradient. When the stress and external field quantities are unknown, the resulting system is fully coupled. For such a case, additional constitutive equations and balance laws (e.g., Maxwell's equations for a magnetomechanical system) are required to complete the mathematical model. However, the focus of this work is on systems, for which the field $\boldsymbol{\mathcal{F}}$ is fully defined, and stress is unknown. We refer to such systems as weakly coupled systems.

In practice, the constitutive relationship (4) is quite nonlinear, and not amenable to a closed form solution for the stress tensor $\mathbf{T}_a$ as a function of strain and field. Hence, when using equation (1) to solve for the displacements, an inversion procedure is inevitable. In what follows, we develop a unified inversion procedure for arbitrary smart materials, and demonstrate its application through magnetostrictive materials.

2.1. Inversion procedure for weakly coupled constitutive model

For convenience, let stress and strain tensors be written in contracted vector notation. For instance, the symmetric stress tensor is written as $\mathbf{T} = [T_1; T_2; T_3; T_4; T_5; T_6]$ with the convention that $T_1 = T_{11}$, $T_2 = T_{22}$, $T_3 = T_{33}$, $T_4 = T_{12}$, $T_5 = T_{23}$, and $T_6 = T_{13}$.

Let $\mathbf{S}(\boldsymbol{\mathcal{F}}, \mathbf{T}) = [S_1; S_2; S_3; S_4; S_5; S_6]$ be a given continuous and differentiable direct model for the strain vector, which takes field and stress vectors as input. Finally, let $\boldsymbol{\mathcal{F}}^*$ and $\mathbf{S}^*$ denote any discrete external field and strain vectors specified from experimental measurements or finite element simulations. The goal of the inverse model is to find the unknown stress vector $\mathbf{T}^*$ that, together with $\boldsymbol{\mathcal{F}}^*$, would give rise to $\mathbf{S}^*$. That is, find $\mathbf{T}$ that satisfies

$$\mathbf{S}(\boldsymbol{\mathcal{F}}^*, \mathbf{T}) - \mathbf{S}^* = 0. \tag{5}$$

Our approach to solving the foregoing equation is based on the Newton method. We expand the direct strain model **S** in a first order Taylor's series as

$$\mathbf{S}(\mathcal{F}, \mathbf{T} + \Delta\mathbf{T}) \approx \mathbf{S}(\mathcal{F}, \mathbf{T}) + \overbrace{\frac{\partial \mathbf{S}(\mathcal{F}, \mathbf{T})}{\partial \mathbf{T}}}^{\mathbf{J}} \Delta\mathbf{T}, \tag{6}$$

where $\Delta\mathbf{T}$ is an incremental stress vector, and **J** is the Jacobian matrix. To find **T**, we employ the foregoing equation, and write a recursive formula based on the Newton method as

$$\mathbf{T}(i+1) \approx \mathbf{T}(i) + \left[\frac{\partial \mathbf{S}(\mathcal{F}^*, \mathbf{T}(i))}{\partial \mathbf{T}}\right]^{-1} (\mathbf{S}^* - \mathbf{S}(\mathcal{F}^*, \mathbf{T}(i)), \tag{7}$$

where i is the iteration index. When the Jacobian terms are known, the algorithm initiates at given start solution stress vector $\mathbf{T}(0)$, and gets corrected in successive iterations, until the algorithm is terminated when the residual error is below a predetermined threshold. At this point, $\mathbf{T}^*$ is obtained.

Calculation of the iterative formula (7) hinges on the material Jacobian of the direct model $\mathbf{S}(\mathcal{F}, \mathbf{T})$, which is material specific. In what follows, we demonstrate the application of this iterative formula to magnetostrictive materials due to their inherent nonlinearity. We give a brief review of the discrete energy-averaged model for Galfenol, and derive its Jacobian terms analytically as required for calculation of the inverse model.

3. Review of calculation of 3D magnetostriction and magnetic flux density for Galfenol

Tari *et al* [29] presented an exact solution procedure for a reformulation of the discrete energy-averaged model, proposed by Evans and Dapino [25], that computes the macroscopic 3D magnetic flux density **B** and strain **S** by minimizing the Gibbs free energy that is defined locally about each easy crystallographic direction. Magnetocrystalline (anisotropy), magnetoelastic (magnetomechanical coupling), and magnetic field (Zeeman) energies constitute the Gibbs free energy in the vicinity of the kth easy direction written as

$$\begin{aligned} \overset{k}{G} &= \frac{1}{2}\,\overset{k}{\mathbf{m}} \cdot \mathbf{K}\,\overset{k}{\mathbf{m}} - (K\,\overset{k}{\mathbf{c}} + \mu_0 M_s \mathbf{H}) \cdot \overset{k}{\mathbf{m}} + \overset{k}{K}_0, \\ k &\in \pm\left\{1, \ldots, \frac{r}{2}\right\}, \end{aligned} \tag{8}$$

where K and K_0 are anisotropy energy constants; $\mathbf{m} = [m_1; m_2; m_3]$ is the magnetization direction having unit magnitude; r is the number of easy crystallographic directions (**c**: the $\langle 100\rangle$ family of six directions for Galfenol); μ_0 and M_s are, respectively, the vacuum permeability and saturation magnetization; and the magnetic stiffness matrix is given by

$$\mathbf{K} = -3\begin{bmatrix} \lambda_{100}T_1 & \lambda_{111}T_4 & \lambda_{111}T_6 \\ \lambda_{111}T_4 & \lambda_{100}T_2 & \lambda_{111}T_5 \\ \lambda_{111}T_6 & \lambda_{111}T_5 & \lambda_{100}T_3 \end{bmatrix}, \tag{9}$$

where λ_{100} and λ_{111} are magnetostriction constants.

The macroscopic 3D strain vector is defined as weighted sums of the response due to the r minimum energy directions as

$$\mathbf{S} = \mathbf{s}\mathbf{T} + \overline{\boldsymbol{\lambda}} = \mathbf{s}\mathbf{T} + \sum_{k=\pm 1}^{\pm r/2} \overset{k}{\xi}_{\text{hys}}\,\overset{k}{\boldsymbol{\lambda}}, \tag{10}$$

where $\overset{k}{\xi}_{\text{hys}}$ and $\overset{k}{\boldsymbol{\lambda}}$ denote, respectively, the averaged hysteretic volume fraction and the magnetostriction tensor written in vector notation for the kth domain; **s** stands for the 6×6 mechanical compliance matrix. Letting Ω be a smoothing factor, the former is calculated as a Boltzmann-type, energy-weighted average as

$$\overset{k}{\xi}_{\text{hys}} = \frac{\exp\left(-\frac{\overset{k}{G}}{\Omega}\right)}{\sum_{n=\pm 1}^{\pm r/2} \exp\left(-\frac{\overset{n}{G}}{\Omega}\right)}, \tag{11}$$

and the magnetostriction tensor components are given as

$$\begin{aligned} \overset{k}{\lambda}_{uu} &= \frac{3}{2}\lambda_{100}(\overset{k}{m}_u \overset{k}{m}_u - c_0), \\ \overset{k}{\lambda}_{uv} &= 3\lambda_{111}\overset{k}{m}_u \overset{k}{m}_v, \quad u \neq v, \end{aligned} \tag{12}$$

where $u, v \in \{1, 2, 3\}$, and c_0 is a nondimensional phenomenological parameter.

The unit magnitude, minimum energy directions $\overset{k}{\mathbf{m}}$ are calculated from the inhomogeneous eigenvalue problem

$$(\mathbf{K} - \overset{k}{\gamma}\,\mathbf{I})\overset{k}{\mathbf{m}} = K\,\overset{k}{\mathbf{c}} + \mu_0 M_s \mathbf{H}, \tag{13a}$$

$$\overset{k}{\mathbf{m}} \cdot \overset{k}{\mathbf{m}} = 1, \tag{13b}$$

where $\overset{k}{\gamma}$ is the unknown Lagrange multiplier corresponding to the kth minimum energy direction.

Letting **Q** be the orthogonal matrix containing the eigenvectors of **K** (with the eigenvalues λ_1, λ_2, and λ_3), Tari *et al* [29] reported that

$$\overset{k}{\mathbf{m}} = \mathbf{Q}\begin{bmatrix} \frac{1}{\lambda_1 - \overset{k}{\gamma}} & 0 & 0 \\ 0 & \frac{1}{\lambda_2 - \overset{k}{\gamma}} & 0 \\ 0 & 0 & \frac{1}{\lambda_3 - \overset{k}{\gamma}} \end{bmatrix}\mathbf{Q}^{\mathrm{T}}(K\,\overset{k}{\mathbf{c}} + \mu_0 M_s \mathbf{H}), \tag{14}$$

where $\overset{k}{\gamma}$ is obtained from the sixth-order polynomial:

$$\begin{aligned} &\overset{k}{\gamma}{}^6 + 2(\bar{\lambda}_2 + \bar{\lambda}_3)\overset{k}{\gamma}{}^5 + (\bar{\lambda}_2^2 + 4\bar{\lambda}_2\bar{\lambda}_3 + \bar{\lambda}_3^2 - \bar{Q}_1 \\ &\quad - \bar{Q}_2 - \bar{Q}_3)\overset{k}{\gamma}{}^4 + 2(\bar{\lambda}_2^2\bar{\lambda}_3 + \bar{\lambda}_2\bar{\lambda}_3^2 - \bar{\lambda}_2\bar{Q}_1 \\ &\quad - \bar{\lambda}_3\bar{Q}_1 - \bar{\lambda}_3\bar{Q}_2 - \bar{\lambda}_2\bar{Q}_3)\overset{k}{\gamma}{}^3 + (\bar{\lambda}_2^2\bar{\lambda}_3^2 - \bar{\lambda}_2^2\bar{Q}_1 \\ &\quad - 4\bar{\lambda}_2\bar{\lambda}_3\bar{Q}_1 - \bar{\lambda}_3^2\bar{Q}_1 - \bar{\lambda}_3^2\bar{Q}_2 - \bar{\lambda}_2^2\bar{Q}_3)\overset{k}{\gamma}{}^2 \\ &\quad - 2\bar{\lambda}_2\bar{\lambda}_3\bar{Q}_1(\bar{\lambda}_2 + \bar{\lambda}_3)\overset{k}{\gamma} - \bar{\lambda}_2^2\bar{\lambda}_3^2\bar{Q}_1 = 0, \end{aligned} \tag{15}$$

with $\overset{k}{\gamma} = \lambda_1 - \overset{k}{\gamma}$, $\bar{\lambda}_2 = \lambda_2 - \lambda_1$, $\bar{\lambda}_3 = \lambda_3 - \lambda_1$, and $[\sqrt{\bar{Q}_1}; \sqrt{\bar{Q}_2}; \sqrt{\bar{Q}_3}] = \mathbf{Q}^{\mathrm{T}}(K\,\overset{k}{\mathbf{c}} + \mu_0 M_s \mathbf{H})$.

When equation (15) has multiple real solutions, the one that results in the lowest Gibbs energy is selected.

4. Strain Jacobian components

The inverse model, developed in section 2.1, requires strain Jacobian terms. In this section, we derive the Jacobian terms for the direct model discussed in section 3. For convenience, the derivative components are derived in indicial with the subscript $i \in \{1, \ldots, 6\}$.

Differentiating equation (10) with respect to T_i gives,

$$\frac{\partial \mathbf{S}}{\partial T_i} = \mathbf{s}\,\overset{i}{\mathbf{e}} + \sum_{k=\pm 1}^{\pm r/2} \frac{\partial \overset{k}{\xi}_{\text{hys}}}{\partial T_i} \overset{k}{\boldsymbol{\lambda}} + \sum_{k=\pm 1}^{\pm r/2} \overset{k}{\xi}_{\text{hys}} \frac{\partial \overset{k}{\boldsymbol{\lambda}}}{\partial T_i}, \tag{16}$$

where $\overset{i}{\mathbf{e}}$ is the six-dimensional unit vector with one as its ith component; the derivative of the averaged hysteretic volume fractions is found from differentiating equation (11) which after simplification may be written as

$$\frac{\partial \overset{k}{\xi}_{\text{hys}}}{\partial T_i} = \frac{1}{\Omega} \overset{k}{\xi}_{\text{hys}} \left(\overset{k}{\boldsymbol{\lambda}}_i - \sum_{n=\pm 1}^{\pm r/2} \overset{n}{\xi}_{\text{hys}} \overset{n}{\boldsymbol{\lambda}}_i \right), \tag{17}$$

and the derivative of the magnetostriction in the direction of the kth easy axis is found from equation (12) as

$$\frac{\partial \overset{k}{\boldsymbol{\lambda}}_{uu}}{\partial T_i} = 3\lambda_{100}\, \overset{k}{m}_u \frac{\partial \overset{k}{m}_u}{\partial T_i},$$
$$\frac{\partial \overset{k}{\boldsymbol{\lambda}}_{uv}}{\partial T_i} = 3\lambda_{111} \left(\overset{k}{m}_u \frac{\partial \overset{k}{m}_v}{\partial T_i} + \overset{k}{m}_v \frac{\partial \overset{k}{m}_u}{\partial T_i} \right), \quad u \neq v.$$

Finally, differentiating the inhomogeneous eigenvalue problem (13) with respect to stress, and solving the resulting equations for the emerging unknown derivatives, one obtains

$$\frac{\partial \overset{k}{\mathbf{m}}}{\partial T_i} = [\mathbf{K} - \overset{k}{\gamma}\,\mathbf{I}]^{-1} \left(\frac{\partial \overset{k}{\gamma}}{\partial T_i} \overset{k}{\mathbf{m}} - \frac{\partial \mathbf{K}}{\partial T_i} \overset{k}{\mathbf{m}} \right), \tag{18}$$

and

$$\frac{\partial \overset{k}{\gamma}}{\partial T_i} = \frac{\frac{\partial \mathbf{K}}{\partial T_i} \overset{k}{\mathbf{m}} \cdot [\mathbf{K} - \overset{k}{\gamma}\mathbf{I}]^{-1} \overset{k}{\mathbf{m}}}{\overset{k}{\mathbf{m}} \cdot [\mathbf{K} - \overset{k}{\gamma}\mathbf{I}]^{-1} \overset{k}{\mathbf{m}}}, \tag{19}$$

which after a simplification procedure can be combined as

$$\frac{\partial \overset{k}{\mathbf{m}}}{\partial T_i} = \frac{|\mathbf{K} - \overset{k}{\gamma}\mathbf{I}|^{-1}}{\overset{k}{\mathbf{m}} \cdot [\mathbf{K} - \overset{k}{\gamma}\mathbf{I}]^{-1} \overset{k}{\mathbf{m}}} \overset{k}{\mathbf{m}} \times \left[[\mathbf{K} - \overset{k}{\gamma}\mathbf{I}] \left(\overset{k}{\mathbf{m}} \times \frac{\partial \mathbf{K}}{\partial T_i} \overset{k}{\mathbf{m}} \right) \right], \tag{20}$$

where '| |' stands for the matrix determinant; '·' and '×' are, respectively, vector dot and cross product operators. Note that the derivative of the stiffness matrix with respect to stress is directly available from equation (9).

5. Reduced 2D system model for embedded smart composites

The computational efficiency of the inverse model is further improved by reducing the 3D system model described in section 2 to a 2D model for thin composite plate structures. For the analysis of thin composite plates, the conventional modeling approach is based on equivalent single layer theories, which are derived from 3D continuum theories by making suitable assumptions concerning the kinematics of deformation or the stress state through the thickness of the laminate. These theories allow the reduction of a 3D problem to a suitable 2D problem [39]. The simplest form of laminate plate theory is the classical plate theory, where the time-dependent 3D cartesian displacements are approximated using asymptotic expansion along the thickness (z-direction), i.e.,

$$u(x, y, z, t) = u_0(x, y, t) + z\phi_x(x, y, t), \tag{21a}$$

$$v(x, y, z, t) = v_0(x, y, t) + z\phi_y(x, y, t), \tag{21b}$$

$$w(x, y, z, t) = w_0(x, y, t), \tag{21c}$$

which reduces the dependence of displacement components u, v, and w to 2D. Here, u_0, v_0, and w_0 are the leading order displacement terms; and ϕ_x and ϕ_y denote rotations about the y and x axes, respectively. Assuming that the deformation has only bending and in-plane stretching components (i.e., transverse normal and transverse shear effects are negligible), these rotations are represented as

$$\phi_x = -\frac{\partial w_o}{\partial x}, \qquad \phi_y = -\frac{\partial w_o}{\partial y}. \tag{22}$$

As the thickness increases, higher order approximations need to be considered. However, classical plate theories work well for composite plates with small thickness ratios ($r \leqslant 0.1$) [34]. Considering this assumption, the displacement forms described by equations (21)–(22) constitute a reduced plane strain problem, in which the strain components S_{zz}, S_{xz}, and S_{yz} are neglected. The remaining strain components can be written as

$$\begin{bmatrix} S_{xx} \\ S_{yy} \\ S_{xy} \end{bmatrix} = \begin{bmatrix} S_{xx}^{(0)} \\ S_{yy}^{(0)} \\ S_{xy}^{(0)} \end{bmatrix} + z \begin{bmatrix} S_{xx}^{(1)} \\ S_{yy}^{(1)} \\ S_{xy}^{(1)} \end{bmatrix}, \tag{23}$$

where

$$S_{xx}^{(0)} = \frac{\partial u_0}{\partial x}, \quad S_{yy}^{(0)} = \frac{\partial v_0}{\partial y}, \quad S_{xy}^{(0)} = \frac{1}{2}\left(\frac{\partial u_0}{\partial y} + \frac{\partial v_0}{\partial x} \right),$$
$$S_{xx}^{(1)} = \frac{\partial \phi_x}{\partial x}, \quad S_{yy}^{(1)} = \frac{\partial \phi_y}{\partial y}, \quad S_{xy}^{(1)} = \frac{1}{2}\left(\frac{\partial \phi_x}{\partial y} + \frac{\partial \phi_y}{\partial x} \right). \tag{24}$$

The variational form for 2D plate theory is derived by substituting stress, displacement, and strain expressions (21)–(24) into 3D Navier's equation (1) as

$$\int_{\tau}\left\{\int_{\Omega_e}\left[\left(\bar{\rho}_o\frac{\partial^2 u_o}{\partial t^2}+\bar{c}_o\frac{\partial u_o}{\partial t}+\bar{\rho}_1\frac{\partial^2\phi_x}{\partial t^2}+\bar{c}_1\frac{\partial\phi_x}{\partial t}\right)\delta u_o\right.\right.$$
$$+\left(\bar{\rho}_o\frac{\partial^2 v_o}{\partial t^2}+\bar{c}_o\frac{\partial v_o}{\partial t}+\bar{\rho}_1\frac{\partial^2\phi_y}{\partial t^2}+\bar{c}_1\frac{\partial\phi_y}{\partial t}\right)\delta v_o$$
$$+\left(\bar{\rho}_o\frac{\partial^2 w_o}{\partial t^2}+\bar{c}_o\frac{\partial w_o}{\partial t}\right)\delta w_o$$
$$+\left(\bar{\rho}_1\frac{\partial^2 u_o}{\partial t^2}+\bar{c}_1\frac{\partial u_o}{\partial t}+\bar{\rho}_2\frac{\partial^2\phi_x}{\partial t^2}+\bar{c}_2\frac{\partial\phi_x}{\partial t}\right)\delta\phi_x$$
$$+\left(\bar{\rho}_1\frac{\partial^2 v_o}{\partial t^2}+\bar{c}_1\frac{\partial v_o}{\partial t}+\bar{\rho}_2\frac{\partial^2\phi_y}{\partial t^2}+\bar{c}_2\frac{\partial\phi_y}{\partial t}\right)\delta\phi_y$$
$$+N_{xx}\delta S_{xx}^{(0)}+N_{xy}\delta S_{xy}^{(0)}+N_{yy}\delta S_{yy}^{(0)}+M_{xx}\delta S_{xx}^{(1)}$$
$$\left.+M_{xy}M_{yy}\delta S_{xy}^{(1)}+M_{yy}\delta S_{yy}^{(1)}\right]\mathrm{d}x\,\mathrm{d}y$$
$$-\int_{\partial\Omega_e}\left[\hat{N}_{nn}\delta u_{on}+\hat{N}_{ns}\delta u_{os}-\hat{M}_{nn}\frac{\partial\delta w_o}{\partial n}\right.$$
$$\left.\left.-\hat{M}_{ns}\frac{\partial\delta w_o}{\partial s}+\hat{Q}_n\delta w_o\right]\mathrm{d}s\right\}\mathrm{d}t=0, \tag{25}$$

where Ω_e represents the total plate area; $\partial\Omega_e$ represents the boundary to Ω_e; τ represents the time over which the dynamic system is studied. Also, the density terms ρ_o, ρ_1, and ρ_2, damping coefficient terms c_0, c_1, and c_2, and stress resultants N_{xx}, N_{yy}, N_{xy}, M_{xx}, M_{yy}, and M_{xy} are defined as

$$\bar{\rho}_k=\int_{t_{\mathrm{tot}}}\rho\,z^k\,\mathrm{d}z,\qquad \bar{c}_k=\int_{t_{\mathrm{tot}}}c\,z^k\,\mathrm{d}z,\quad (k=0,\,1,\,2), \tag{26}$$

$$\begin{bmatrix}N_{xx}\\N_{yy}\\N_{xy}\end{bmatrix}=\int_{t_{\mathrm{tot}}}\begin{bmatrix}T_{xx}\\T_{yy}\\T_{xy}\end{bmatrix}\mathrm{d}z, \tag{27}$$

$$\begin{bmatrix}M_{xx}\\M_{yy}\\M_{xy}\end{bmatrix}=\int_{t_{\mathrm{tot}}}\begin{bmatrix}T_{xx}\\T_{yy}\\T_{xy}\end{bmatrix}z\,\mathrm{d}z, \tag{28}$$

where t_{tot} is the total plate thickness, and the boundary terms $\hat{N}_{nn}$, $\hat{N}_{ns}$, $\hat{M}_{nn}$, and $\hat{M}_{ns}$ are the normal and tangential components defined as

$$\begin{bmatrix}\hat{N}_{nn}\\\hat{N}_{ns}\end{bmatrix}=\int_{t_{\mathrm{tot}}}\begin{bmatrix}\hat{\sigma}_{nn}\\\hat{\sigma}_{ns}\end{bmatrix}\mathrm{d}z, \tag{29}$$

$$\begin{bmatrix}\hat{M}_{nn}\\\hat{M}_{ns}\end{bmatrix}=\int_{t_{\mathrm{tot}}}\begin{bmatrix}\hat{\sigma}_{nn}\\\hat{\sigma}_{ns}\end{bmatrix}z\mathrm{d}z,\qquad \hat{Q}_n=\int_{t_{\mathrm{tot}}}\hat{\sigma}_{nz}\mathrm{d}z, \tag{30}$$

with $\hat{\sigma}_{nn}$, $\hat{\sigma}_{ns}$, and $\hat{\sigma}_{nz}$ as the specified stress components on the portion of the boundary $\partial\Omega_e$.

Note that the integrals (26)–(28) can be directly calculated when the geometry and material properties are specified. However, the stress resultant terms are calculated utilizing the inverse model developed in section 2.1.

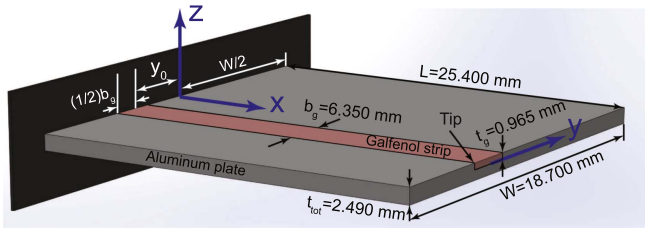

Figure 1. Schematic of a Galfenol-aluminum composite structure. The x–y plane of the coordinate system is coincident with the bottom plane of the Galfenol strip, and the x–z plane is a plane of symmetry ($y_0 = 0$).

In what follows, the aforementioned mathematical framework is applied to a Galfenol-aluminum composite structure, and relevant simulation results are presented.

6. Case study: Galfenol-aluminum structure for actuator applications

Figure 1 depicts a schematic view of a Galfenol-aluminum composite structure. The material parameters for aluminum are: $E = 69$ GPa, $\nu = 0.3$, and $\rho = 2700$ kg m^{-3}; and those for Galfenol are tabulated in table 1.

The actuator geometry presented in this paper mirrors the sample utilized in the experimental set-up presented in [40]. The composite plate actuator, consisting of embedded magnetostrictive domain, was manufactured using ultrasonic additive manufacturing [41]. To obtain a bending actuator configuration, the plate was excited using 1D magnetic fields along the Galfenol length, and cantilevered boundary conditions were imposed at the clamped edge. The input alternating and bias magnetic fields of different amplitudes and frequencies (ranging from 0.1 to 500 Hz) were generated using a conductive coil and the displacement data at the tip of the Galfenol patch (labeled in figure 1) was collected. The measured data was subsequently reproduced within a reasonable tolerance, using a dynamic 2D plate model which employed the inversion procedure presented in [27]. Additionally, this model assumed approximately uniform magnetic fields throughout the Galfenol volume, which is a reasonable assumption for a plate actuator undergoing small deformations.

In what follows, our novel inversion scheme and the 2D plate model developed in sections 2 and 5 are utilized to study the actuator displacements. Through this application, we demonstrate the computational efficiency and numerical robustness of the proposed computational framework through a comparison with the aforementioned existing approach.

6.1. Solution methodology

The actuator system presented in figure 1 is analyzed using the 2D weak form described by equations (25)–(30). The 2D equations are implemented in the finite element software COMSOL Multiphysics (version 4.3b), and the constitutive model for Galfenol along with the inversion scheme presented

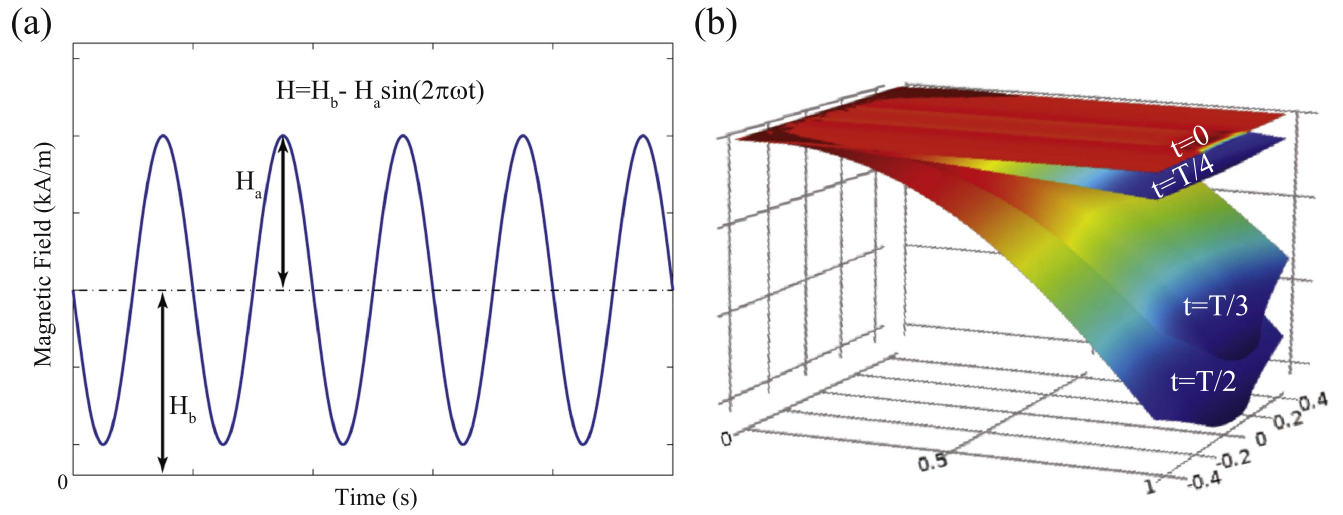

Figure 2. (a) A schematic plot of 1D magnetic field input: $H(t) = H_b - H_a \sin(2\pi\omega t)$, and (b) schematic deflected plate configurations (dimensions in inches) at different fractions of time period (T) corresponding to the frequency ω.

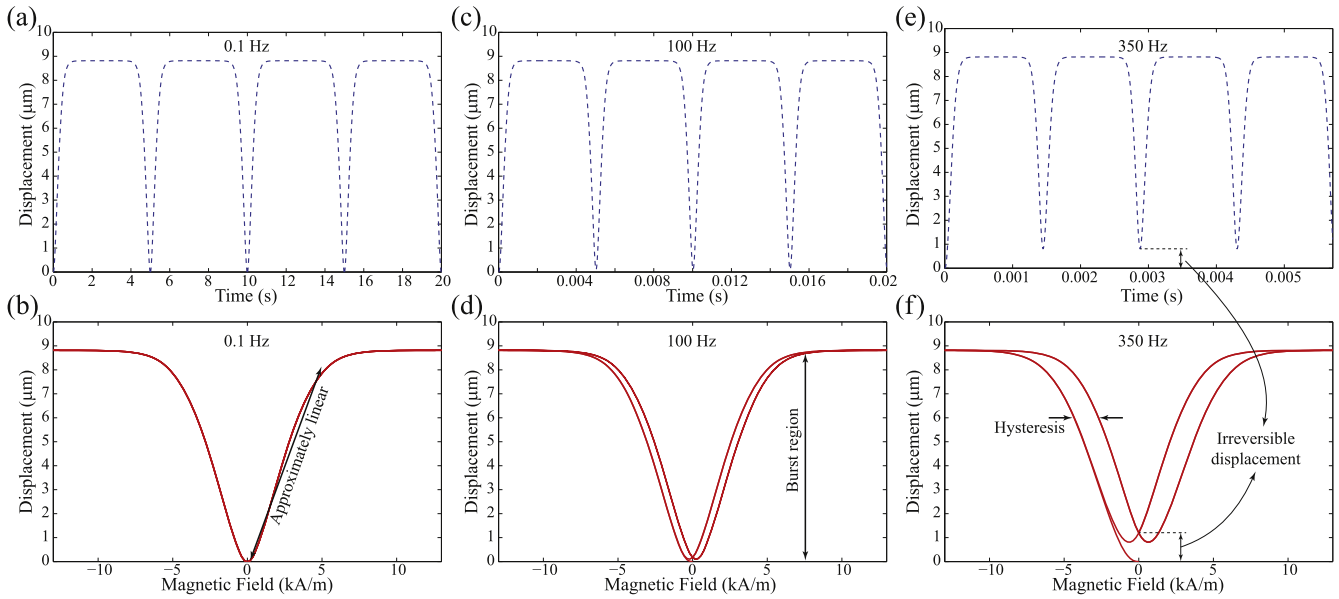

Figure 3. Dynamic actuation results, obtained using the proposed model, with 1D unbiased magnetic field input ($H(t) = -15\sin(2\pi\omega t)$ kA m^{-1}) for two periods at frequencies: (a) and (b) 0.1 Hz; (c) and (d) 100 Hz; and (e) and (f) 350 Hz. The displacement–field curves are for the last period.

in section 2.1 are coded as MATLAB m-files and supplied to COMSOL.

A 1D harmonic magnetic field of the form $H(t) = H_b - H_a \sin(2\pi\omega t)$ is given as input to the system and the displacements at the tip of the Galfenol patch are analyzed. To generate complete magnetostriction curves, unbiased magnetic field input ($H_b = 0$) of amplitude $H_a = 15$ kA m^{-1} greater than the saturation field $H_{\text{sat}} \approx 10$ kA m^{-1} is applied. To obtain the displacement-field minor loops, a biased magnetic field with $H_b = 3.5$ kA m^{-1} and $H_a = 3.25$ kA m^{-1} is supplied as input.

Note that no matter what the input field is, the Galfenol patch elongates, and since the centroid of the patch is placed above the neutral axis of the entire plate, it causes the plate to always deflect downward. This is schematically shown in figure 2(b) for a typical input field. Further results are elaborated in the following section.

6.2. Simulation results

Figure 3 depicts the dynamic actuation simulation results, obtained using the proposed model, with unbiased input magnetic field at various frequencies for two periods. At the lowest frequency (0.1 Hz), as expected, hysteresis is minimal but gets pronounced as the field frequency increases. Hysteresis makes the plate actuator a nonconservative system. To be precise, the displacement vanishes at zero field for both periods as in figures 3(a)–(d). In contrast, as shown in figures 3(e) and (f), there is a nonzero displacement at zero field at nonzero time.

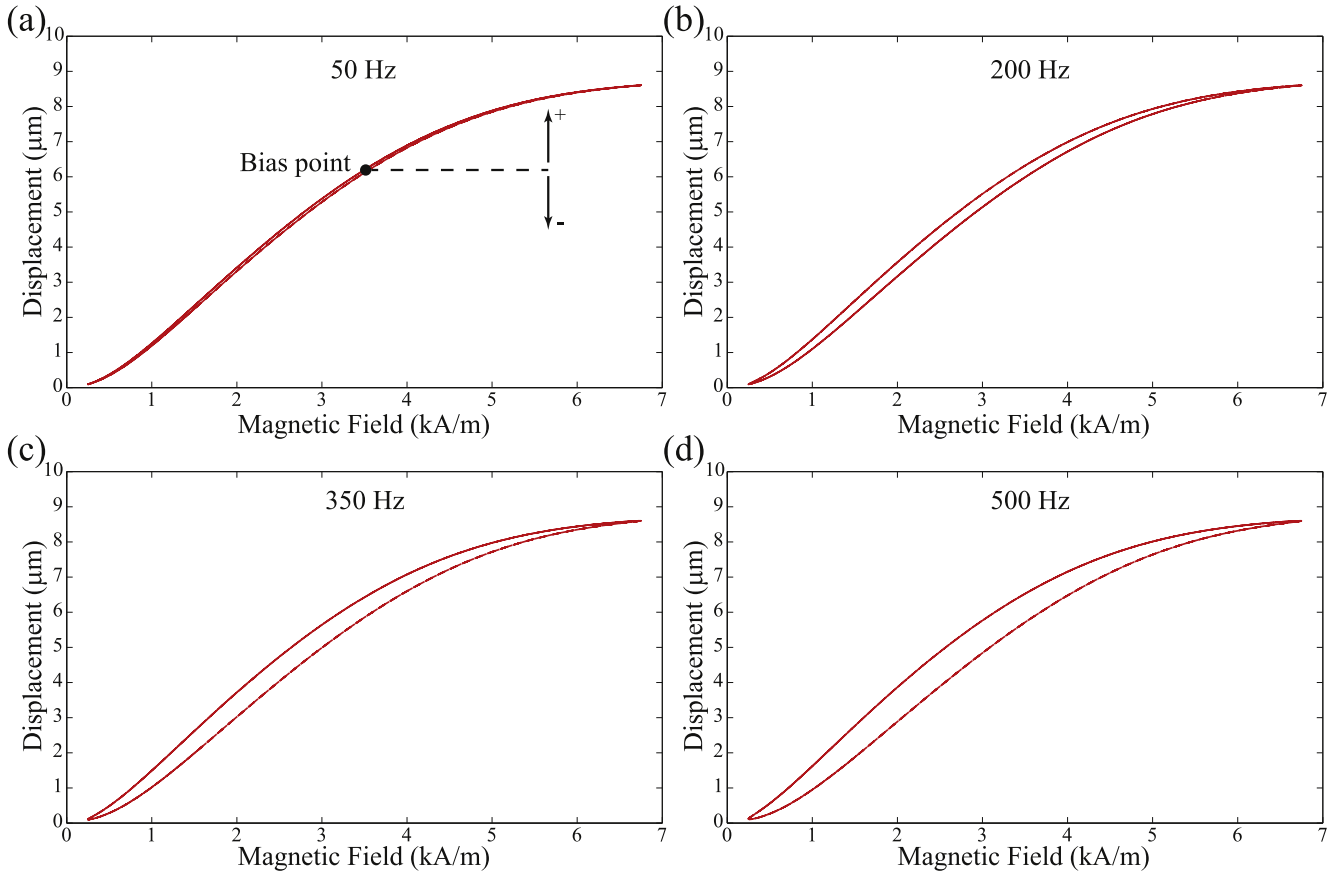

Figure 4. Dynamic actuation results with biased 1D magnetic field input $H(t) = 3.50 - 3.25\sin(2\pi\omega t)$ kA m^{-1} at different frequencies: (a) 50 Hz, (b) 200 Hz, (c) 350 Hz, and (d) 500 Hz.

Table 1. Parameters for the direct model, given in section 3, for Galfenol.

Par.	M_s (kA m^{-1})	E (GPa)	λ_{100} (ppm)	λ_{111} (ppm)	c_0	ρ (kg m^{-3})
Value	1273.24	74.50	173.33	−6.67	0.33	7870.00
Par.	K (kJ m^{-3})	K_{100} (J m^{-3})	Ω (J)	G (GPa)	ν	c (N s m^{-1})
Value	30.00	−250.00	1200.00	120.00	0.30	0.10

In addition, figures 3(b), (d), and (f) show that the plate actuator exhibits an approximately linear response in the 'burst' region, which forms the basis for the early linear formulations for magnetostrictive transducers. Exploiting the linearity can potentially improve the computational efficiency, but would limit the operational regime of the plate actuator. This motivated our nonlinear solution methodology.

The actuator response to bias input at different frequencies are demonstrated in figure 4, in which an appropriate bias field maps the domain of the input field such that the actuator is operating in the burst region for its entire operational regime. As a further advantage, field biasing can produce bi-directional strains about the bias point, while this is not feasible for the unbiased plate actuator.

In what follows, efficiency and effectiveness of the proposed inverse model are compared to those of the existing approach [27]. The same COMSOL framework discussed above is used for both models except that separate MATLAB subroutines for each inverse model are used. Recall that the proposed inverse model employs the inversion scheme presented in section 2.1 along with the exact analytical Jacobian terms developed in section 4 for the constitutive material model reviewed in section 3. In contrast, the existing inverse model employs the quasi-Newton method with approximate Jacobian terms for the constitutive material model presented in [26]. In addition, the maximum allowable number of iterations for the proposed and existing models are taken, respectively, 50 and 500 in the MATLAB subroutines.

6.2.1. Simulation time comparison. The simulation cases discussed above are repeated with the existing inverse model. For all simulations, a physics controlled mesh is used wherein the plate is discretized with triangular mesh elements of size varying from 0.0762 to 0.17018 mm, thus having 5946

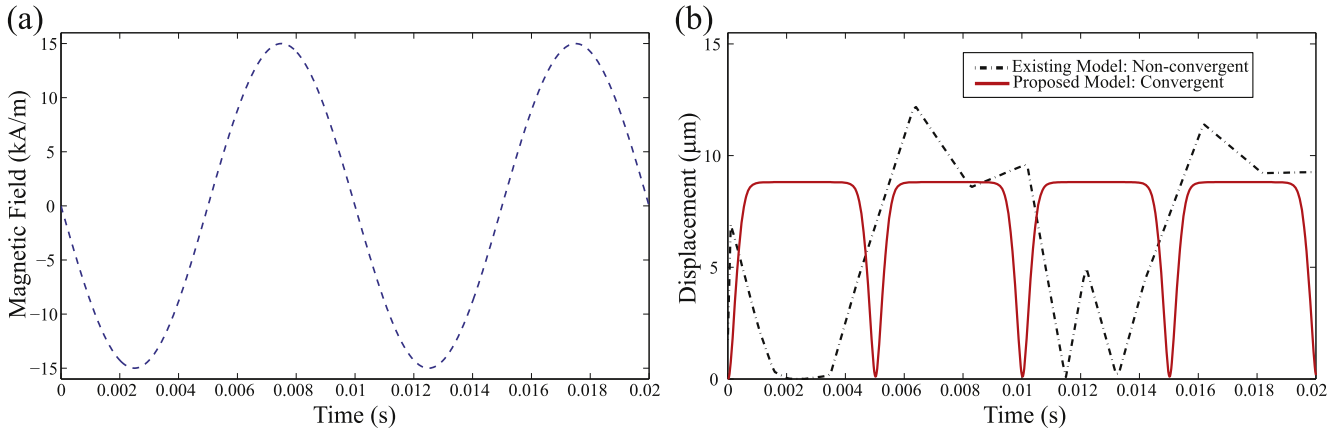

Figure 5. Plots of (a) unbiased 1D harmonic magnetic field input, and (b) the plate's response at the tip at 100 Hz.

DOFs. The simulations were performed on a quad core 64 bit desktop computer, and the runtimes are tabulated in table 2. Note that the static runtimes correspond to the single initial time instant, and the dynamic simulation runtimes correspond to the averaged time taken to complete one periodic cycle for all of the frequencies discussed above.

As per table 2, the proposed inverse model gives dynamic simulation results in almost six times faster than the existing inverse model does. This noticeable time advantage makes the proposed inverse model an effective and efficient tool for the fast design of plate actuators.

6.2.2. Convergence comparison. The proposed model offers a significant improvement in convergence for dynamic simulations. COMSOL solves for the system state at each instant starting from the initial solution, which is the previous system state. We observed that the proposed model is able to handle large variation in response between reasonably large time steps, while the existing model requires a very close estimate of the initial solution. This wider convergence zone is attributed to the employment of the analytical strain derivative terms, developed in section 4, by the proposed model.

The existing model was not convergent for any of the cases shown in figure 3. There are two sources of non-convergence for the existing model. The first source originates from the singularity issues manifested by the material model [26] as pointed out by Tari *et al* [29]. The other source is the employment of approximate Jacobian terms for the material model together with the quasi-Newton technique. This approximation is not sufficient to find the optimal direction for minimizing the residual error in each iteration. For convenience, field input and strain output plots using both models are shown in figure 5 for the unbiased harmonic magnetic field of frequency 100 Hz over a duration of $t = 0.02$ s. The figure demonstrates that the existing model converges to a mathematical solution, which is nonphysical. The inversion scheme in the existing model exhausted the maximum allowable number of iterations (500) and failed to sufficiently minimize the residual error. Thus, the best obtained solution is reported. In contrast, the proposed model only needed 50 iterations to converge and it always converged to the optimal solution within 50 iterations.

Table 2. Simulation runtimes for the existing and proposed models.

Model	Existing	Proposed
Static (hh:mm)	00:09	00:02
Dynamic (hh:mm)	30:06	05:09

6.2.3. Sensitivity to input data. Figure 6 illustrates the plate's response obtained using the proposed model for a non-smooth input field. The existing model performed satisfactorily until $t = 0.02$ s, after which COMSOL's nonlinear simulation solver took too much time to converge to a solution satisfying the non-local Navier equation, so no result is shown. In contrast, the proposed model is robust in the presence of the sharp corner at $t = 0.02$ s, as demonstrated in figure 6(b).

To further benchmark the proposed model, we devised trapezoidal and rectangular periodic magnetic field inputs of 50 Hz shown in figures 7(a) and (c). The plate's responses obtained using the proposed model for the two inputs are depicted in figures 7(b) and (d), respectively. As before, the proposed model is able to converge at the sharp corners.

7. Summary

A computationally efficient and robust nonlinear modeling framework for smart material systems was presented. A new 3D inversion scheme for nonlinear modeling of smart material based transducers, and a reduced 2D model for smart composite plate structures constitute the framework. The framework was integrated with a finite element software to analyze an aluminum plate embedded with a Galfenol strip. For Galfenol, analytical 3D strain derivative terms for a recent model were derived. The resulting nonlinear finite element framework was utilized to obtain major and minor magnetostriction curves corresponding to the tip of the Galfenol

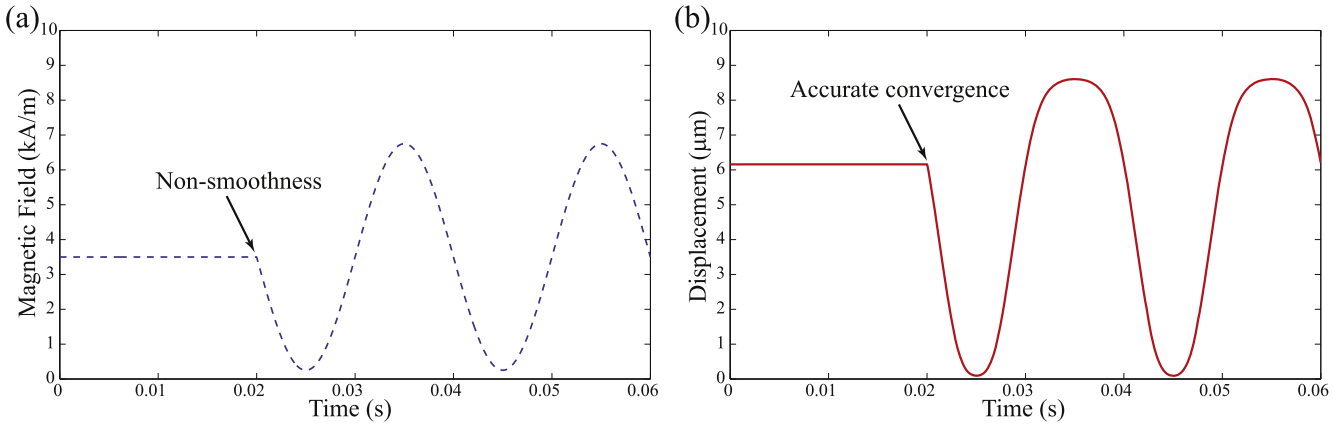

Figure 6. (a) Plot of non-smooth 1D magnetic field input, and (b) the plate's response at the tip obtained using the proposed model.

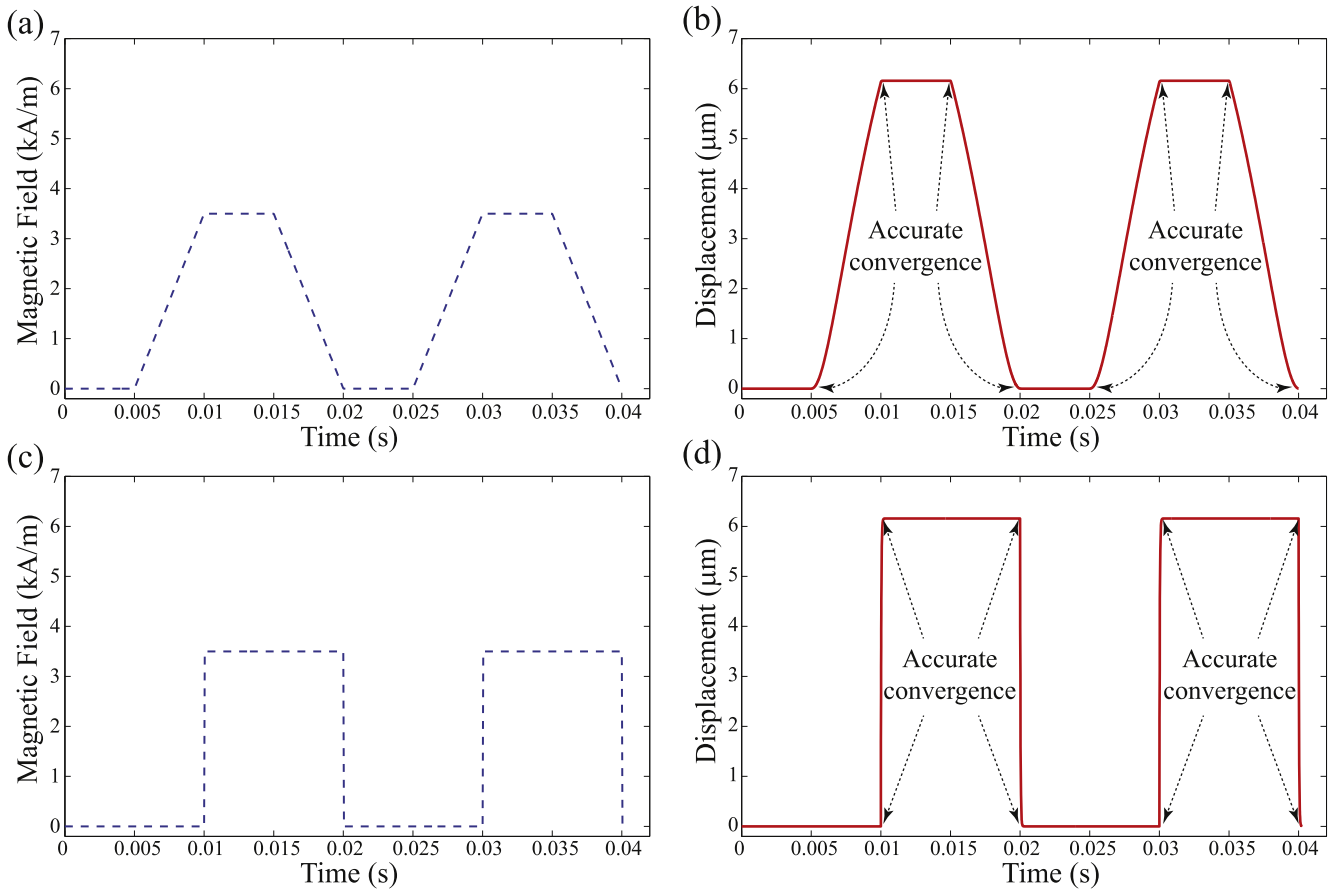

Figure 7. Plots of 1D (a) trapezoidal and (c) rectangular periodic magnetic field inputs at 50 Hz; and (b) and (d) the plate's responses at the tip obtained using the proposed model, respectively.

patch with applying unbiased and biased magnetic fields, respectively. Compared to an existing model, the proposed model gave dynamic simulation results in almost six times faster. Additionally, when an unbiased input field was applied, the proposed model converged accurately to the physical solution, while the existing model converged to a mathematical solution that was nonphysical. The significant advantages in computational time and numerical convergence exhibited by the proposed model are ideal for fast design of plate actuators.

Acknowledgments

The authors wish to acknowledge the financial support from NASA Glenn Research Center and Honda R&D Americas

through the Smart Vehicle Concepts Center (www.SmartVehicleCenter.org) at the Ohio State University.

Appendix A. Derivation of $\frac{\partial \overset{k}{G}}{\partial T_i}$

The derivative of the Gibbs free energy (equation (8)) with respect to stress has a major role in the analytical reduction of the derivative of the volume fractions with respect to stress presented already by equation (17). Therefore, a step by step derivation procedure for such a key term is given as follows.

With letting $tr()$ denote the trace of a matrix, we rewrite the Gibbs free energy given by equation (8) as

$$\overset{k}{G} = \frac{1}{2}\overset{k}{\mathbf{m}} \cdot \mathbf{K}\overset{k}{\mathbf{m}} - (K\overset{k}{\mathbf{c}} + \mu_0 M_s \mathbf{H}) \cdot \overset{k}{\mathbf{m}} + \overset{k}{K_0} + \frac{3}{2}c_0\lambda_{100}\, tr(\mathbf{T}), \quad k \in \pm\left\{1, \ldots, \frac{r}{2}\right\}, \tag{A.1}$$

which leaves the direct model unchanged, as we are shifting the base energy of all of the easy axes the same amount. Differentiating the foregoing equation with respect to stress is given as follows:

$$\begin{aligned}
\frac{\partial \overset{k}{G}}{\partial T_i} &= \frac{\partial \overset{k}{\mathbf{m}}}{\partial T_i} \cdot \mathbf{K}\overset{k}{\mathbf{m}} + \frac{1}{2}\overset{k}{\mathbf{m}} \cdot \frac{\partial \mathbf{K}}{\partial T_i}\overset{k}{\mathbf{m}} \\
&\quad - \frac{\partial \overset{k}{\mathbf{m}}}{\partial T_i} \cdot (K\overset{k}{\mathbf{c}} + \mu_0 M_s \mathbf{H}) + \frac{3}{2}c_0\lambda_{100}\frac{\partial tr(\mathbf{T})}{\partial T_i} \\
&= \frac{\partial \overset{k}{\mathbf{m}}}{\partial T_i} \cdot \mathbf{K}\overset{k}{\mathbf{m}} + \frac{1}{2}\overset{k}{\mathbf{m}} \cdot \frac{\partial \mathbf{K}}{\partial T_i}\overset{k}{\mathbf{m}} \\
&\quad - \frac{\partial \overset{k}{\mathbf{m}}}{\partial T_i} \cdot (\mathbf{K} - \overset{k}{\gamma}\mathbf{I})\overset{k}{\mathbf{m}} + \frac{3}{2}c_0\lambda_{100}\frac{\partial tr(\mathbf{T})}{\partial T_i} \\
&= \frac{1}{2}\overset{k}{\mathbf{m}} \cdot \frac{\partial \mathbf{K}}{\partial T_i}\overset{k}{\mathbf{m}} + \frac{3}{2}c_0\lambda_{100}\frac{\partial tr(\mathbf{T})}{\partial T_i} \\
&= -\begin{Bmatrix} \frac{3}{2}\lambda_{100}(m_i^k m_i^k - c_0), & i \in \{1, 2, 3\} \\ 3\lambda_{111}\overset{k}{m_1}\overset{k}{m_2}, & i = 4 \\ 3\lambda_{111}\overset{k}{m_2}\overset{k}{m_3}, & i = 5 \\ 3\lambda_{111}\overset{k}{m_3}\overset{k}{m_1}, & i = 6 \end{Bmatrix} = -\overset{k}{\lambda_i},
\end{aligned} \tag{A.2a}$$

where we use the identity

$$\frac{\partial \overset{k}{\mathbf{m}}}{\partial T_i} \cdot \overset{k}{\mathbf{m}} = 0, \tag{A.3}$$

which is obtained from differentiating equation (13*b*) with respect to stress.

References

[1] Kwun H and Bartels K A 1998 *Ultrasonics* **36** 171–8
[2] Dosch J J, Inman D J and Garcia E 1992 *J. Intell. Mater. Syst. Struct.* **3** 166–85
[3] Sodano H A, Inman D J and Park G 2004 *Shock Vib. Dig.* **36** 197–206
[4] Chandrashekhara K and Agarwal A N 1993 *J. Intell. Mater. Syst. Struct.* **4** 496–508
[5] Smith R C 2005 *Smart Material Systems: Model Development* vol 32 (Philadelphia: Siam)
[6] Leo D J 2007 *Engineering Analysis of Smart Material Systems* (New York: Wiley-Interscience)
[7] Cady W G 1964 *Piezoelectricity: An Introduction to the Theory and Applications of Electromechanical Phenomena in Crystals* (New York: Dover)
[8] Zhang S Q, Li Y X and Schmidt R 2015 *Compos. Struct.* **126** 89–100
[9] Chakrabarti S and Dapino M J 2012 *J. Appl. Phys.* **111** 054505
[10] Kellogg R A 2003 Development and modeling of iron-gallium alloys *PhD Thesis* Iowa State University
[11] Pérez-Aparicio J L and Sosa H 2004 *Smart Mater. Struct.* **13** 493
[12] Landau L and Lifshitz E 1935 *Phys. Z. Sowjetunion* **8** 153
[13] Wang X P, García-Cervera C J and Weinan E 2001 *J. Comput. Phys.* **171** 357–72
[14] García-Cervera C J, Gimbutas Z and Weinan E 2003 *J. Comput. Phys.* **184** 37–52
[15] de Wiele B V, Olyslager F and Dupré L 2008 *J. Comput. Phys.* **227** 9913–32
[16] Preisach F 1935 *Z. Phys.* **94** 277–302
[17] Globus A 1975 *Proc. Europ. Physical Society, Conf. on Soft Magnetic Material* vol 2, p 233
[18] Jiles D C and Atherton D L 1986 *J. Magn. Magn. Mater.* **61** 48–60
[19] Stoner E C and Wohlfarth E P 1991 *IEEE Trans. Magn.* **27** 3475–518
[20] Liorzou F, Phelps B and Atherton D L 2000 *IEEE Trans. Magn.* **36** 418–28
[21] Carman G P and Mitrovic M 1995 *J. Intell. Mater. Syst. Struct.* **6** 673–83
[22] Zheng X J and Sun L 2006 *J. Appl. Phys.* **100** 063906
[23] Armstrong W D 2003 *J. Magn. Magn. Mater.* **263** 208–18
[24] Atulasimha J, Akhras G and Flatau A B 2008 *J. Appl. Phys.* **103** 07B336
[25] Evans P G and Dapino M J 2010 *J. Appl. Phys.* **107** 063906
[26] Chakrabarti S 2011 Modeling of 3D magnetostrictive systems with application to Galfenol and Terfenol-D transducers *PhD Thesis* The Ohio State University
[27] Chakrabarti S and Dapino M J 2011 *Smart Mater. Struct.* **20** 105034
[28] Deng Z and Dapino M J 2013 *Proc. SPIE* **8689** 86890V
[29] Tari H, Scheidler J J and Dapino M J 2015 *J. Magn. Magn. Mater.* **384** 266–75
[30] Evans P G and Dapino M J 2011 *IEEE Trans. Magn.* **47** 221–30
[31] Huber J E, Fleck N A, Landis C M and McMeeking R M 1999 *J. Mech. Phys. Solids* **47** 1663–97
[32] Boyd J G and Lagoudas D C 1996 *Int. J. Plast.* **12** 805–42
[33] Mindlin R D 1972 *Int. J. Solids Struct.* **8** 895–906
[34] Reddy J N 1999 *Eng. Struct.* **21** 568–93
[35] Kannan K S and Dasgupta A 1997 *Smart Mater. Struct.* **6** 341
[36] Datta S, Atulasimha J, Mudivarthi C and Flatau A B 2008 *Smart Mater. Struct.* **17** 025010
[37] Datta S, Atulasimha J, Mudivarthi C and Flatau A B 2009 *J. Intell. Mater. Syst. Struct.* **20** 1121–35
[38] Shu L, Headings L, Dapino M J, Chen D and Lu Q 2013 *J. Intell. Mater. Syst. Struct.* **0** 1–17
[39] Reddy J N 2003 *Mechanics of Laminated Composite Plates and Shells: Theory and Analysis* (Boca Raton, FL: CRC)
[40] Santapuri S, Scheidler J J and Dapino M J 2015 *Compos. Struct.* **132** 737–45
[41] Graff K F 2011 Ultrasonic additive manufacturing *ASM Handbook 6A* (*Welding Fundamentals and Processes*) (ASM Int'l) p 731